HHS Public Access

Author manuscript

Neuroimage. Author manuscript; available in PMC 2020 December 22.

Published in final edited form as:

Neuroimage. 2020 October 15; 220: 117047. doi:10.1016/j.neuroimage.2020.117047.

Connectivity dynamics from wakefulness to sleep

Eswar Damaraju[a,b,*], **Enzo Tagliazucchi**[c], **Helmut Laufs**[d,e], **Vince D Calhoun**[a,b]

[a]Tri-Institutional Center for Translational Research in Neuroimaging and Data Science (TReNDS), Atlanta, GA

[b]Department of Electrical and Computer Engineering, Georgia Institute of Technology, Atlanta, USA

[c]Departamento de Física, Universidad de Buenos Aires, Buenos Aires, Argentina

[d]Department of Neurology and Brain Imaging Center, Goethe University Frankfurt am Main, Germany

[e]Department of Neurology, Christian Albrechts University, Kiel, Germany

Abstract

Interest in time-resolved connectivity in fMRI has grown rapidly in recent years. The most widely used technique for studying connectivity changes over time utilizes a sliding windows approach. There has been some debate about the utility of shorter versus longer windows, the use of fixed versus adaptive windows, as well as whether observed resting state dynamics during wakefulness may be predominantly due to changes in sleep state and subject head motion. In this work we use an independent component analysis (ICA)-based pipeline applied to concurrent EEG/fMRI data collected during wakefulness and various sleep stages and show: 1) connectivity states obtained from clustering sliding windowed correlations of resting state functional network time courses well classify the sleep states obtained from EEG data, 2) using shorter sliding windows instead of longer non-overlapping windows improves the ability to capture transition dynamics even at windows as short as 30 seconds, 3) motion appears to be mostly associated with one of the states rather than spread across all of them 4) a fixed tapered sliding window approach outperforms an adaptive dynamic conditional correlation approach, and 5) consistent with prior EEG/fMRI work, we identify evidence of multiple states within the wakeful condition which are able to be classified with high accuracy. Classification of wakeful only states suggest the presence of time-varying changes in connectivity in fMRI data beyond sleep state or motion. Results also inform about advantageous technical choices, and the identification of different clusters within wakefulness that are separable suggest further studies in this direction.

1. Introduction

The human brain continuously engages in mental activities that include introspection, theory of mind, and future planning, even when not actively pursuing a task. Fluctuations during the resting state have been shown to show functional network topology similar to that

*Corresponding author edamaraju@gsu.edu (Eswar Damaraju).

observed in task imaging studies (Calhoun et al., 2008; Smith et al., 2009). Since the first reports on time varying functional connectivity during task performance (Sakoğlu et al., 2010) and during a typical resting functional magnetic resonance imaging (fMRI) scan (Chang and Glover, 2010; Sakoğlu et al., 2010), there has been interest in studying and characterizing the changes in functional connectivity between brain regions on a shorter time scale, also referred to as time-resolved or dynamic functional connectivity(Calhoun et al., 2014; Hutchison et al., 2013). Recent years have seen a sharp increase in development of novel methods to characterize these dynamics (Allen et al., 2012a; Cribben et al., 2013; Kang et al., 2011; Tagliazucchi et al., 2012a; Vidaurre et al., 2017; Yaesoubi et al., 2015a) (see (Preti et al., 2017) for a thorough review).

One popular method to estimate connectivity dynamics in functional neuroimaging data is the use of sliding windows to estimate the connectivity between regions/networks. These time-varying connectivity estimates, when computed on the time courses from brain regions or seeds defined a priori are referred to as dynamic functional connectivity (dFC) and those estimated from the time courses of networks obtained from blind decomposition techniques such as independent components analysis (ICA) are referred to as dynamic functional network connectivity (dFNC). In this work we focus on the latter, which leverages the benefits of ICA including data-driven identification of networks, robustness to noise, separation of overlapping signals of interest, and estimation of homogeneous networks that capture individual subject variability (Calhoun and de Lacy, 2017; Yu et al., 2017). Using an ICA based pipeline, Allen et al. (2012a) reported the presence of stable, recurring connectivity patterns/states obtained from clustering pairwise correlation estimates of windowed time courses of ICA derived intrinsic networks from resting fMRI data and more recently (Abrol et al., 2017) showed connectivity patterns and dynamic metrics are highly replicable across multiple independent data sets. However, a few studies have raised concerns over the quality of connectivity estimates obtained using the sliding window method (Lindquist et al., 2014; Smith et al., 2011), choice of window size (Hindriks et al., 2016; Leonardi and Van De Ville, 2015; Sakoğlu et al., 2010; Zalesky and Breakspear, 2015), and the ability of the method to capture meaningful state transitions (Shakil et al., 2016). Others have primarily attributed the observable changes in connectivity in resting fMRI data to sleep state Chang et al. (2016); Tagliazucchi and Laufs (2014); Haimovici et al. (2017), sampling variability and head motion (Laumann et al., 2016; Liegeois et al., 2017).

In our prior concurrent EEG/fMRI work (Allen et al., 2017), windows corresponding to distinct dFNC connectivity states estimated using a sliding-window correlation method were associated with distinct electrophysiological signatures during both eyes open and eyes closed awake conditions and showed the ability of the method to track subject vigilance. However, since subjects were mostly awake throughout the scan sessions, simultaneously acquired electroencephalogram (EEG) data did not show enough state transitions from wakefulness to assess how well observed dFNC state transitions correspond to neurobiological state transitions i.e. observable changes in subject sleep state from EEG data.

Here we use simultaneous EEG-resting fMRI data collected continuously over 50 minutes while the subjects transitioned between wakefulness and different sleep stages (defined by EEG-based sleep scoring) and assessed the ability of sliding window based dFNC measures to track the changes across these different wakefulness states. In addition to comparing the dFNC measure to sleep, this study provides us an opportunity to evaluate the impact of several technical choices within a real world dataset rather than in simulations (Leonardi and Van De Ville, 2015; Sakoğlu et al., 2010). For example, we compare the impact of the length of the sliding window, precisely tapered sliding window (Allen et al., 2012a; Barttfeld et al., 2015; Yaesoubi et al., 2015b; Zalesky et al., 2014), on our ability to predict sleep stage. Windows should be short enough to be a good compromise between the ability to capture time varying connectivity without being too sensitive to noise. In addition, we compare a 'fixed length' sliding window approach to a method from econometrics which has been applied to fMRI data, the dynamic conditional correlation (DCC) (Engle, 2002; Lindquist et al., 2014). DCC uses an adaptive window size and has been reported to show better test-rest reliability compared to 'fixed length' sliding-window methods in estimating time varying functional connectivity (Choe et al., 2017). We also evaluate the relationship of the estimated states to motion, in particular we were interested in whether all states would show a similar relationship to motion or whether a subset of states captures the variance associated with motion.

2. Methods

2.1. Data acquisition

Resting state functional MRI data was collected from 55 subjects for 52 minutes each (1505 volumes of echo planar images, repetition time (TR)=2.08 s, TE = 30 ms, matrix 64 × 64; FOV = 192 mm^2, Thickness=2 mm, 1 mm gap between slices) on a Siemens 3T Trio scanner while the subjects rested with their eyes closed (details in (Tagliazucchi et al., 2012b)). Simultaneous EEG was acquired on 30 EEG channels with FCz as the reference (sampling rate = 5 kHz, low pass filter = 250 Hz, high pass filter = 0.016 Hz) using an MR compatible device (BrainAmp MR+, BrainAmp ExG; Brain Products, Gilching, Germany).

Of 63 nonsleep-deprived subjects scanned in the evening after 8:00 PM, 8 subjects had no epochs of sleep and were not used in this analysis. Remaining 55 subjects reached at least sleep stage N1 as assessed from EEG derived hypnogram and were included in the analysis. All subjects reached at least N1 sleep stage, 39 reached N2 stage and 19 went into N3 stage during the scan. For details of epochs of individual sleep durations, see Supplemental Table 7.1 of Tagliazucchi et al. (2013).

2.2. Data preprocessing

EEG data underwent MRI and pulse artifact correction based on average artifact subtraction (Allen et al., 1998), followed by ICA-based residual artifact rejection. This data was subsequently sleep staged into wakeful (W), drowsy/light sleep (N1), moderate sleep (N2), and deep sleep (N3) stages by a sleep expert per American Academy of Sleep Medicine (AASM) criteria (AASM and Iber, 2007) resulting in a hypnogram for the scan duration for each subject. None of the participants went into REM sleep stage during the scan period.

The first 5 volumes of functional imaging data were discarded to account for T1 equilibration effects. The data were then corrected for head movement (rigid body) and slice timing differences. Subject data was then spatially normalized to MNI template space using SPM12 toolbox and resampled to 3 mm^3 isotropic voxel resolution. Since the scan duration was long, we detrended each voxel time series using a high model order (21) polynomial. The subject brain voxel data were then spatially smoothed to 5 mm FWHM using AFNI's 3dBlurInMask. Finally, the voxel time courses were variance normalized (z-scored).

2.3. Independent component estimation

We performed a group independent component analysis (Calhoun et al., 2001; Calhoun and Adali, 2012) using the GIFT toolbox (http://mialab.mrn.org/software/gift) to decompose the data into 100 spatially independent components each associated with a coherent time course. First subject data were reduced in time to 1400 points using principal components analysis (PCA). These time reduced datasets were then concatenated in time and a group PCA was used to further reduce the data to 100 orthogonal directions of maximal variance. Spatial ICA analysis was performed on this data to obtain 100 spatially independent components using infomax algorithm. To ensure stability of decomposition, the Infomax ICA algorithm was repeated 20 times in ICASSO (Himberg et al., 2004) with random initialization, and aggregate spatial maps were estimated as the modes of the component clusters. Subject specific component maps and their associated time courses were obtained using spatio-temporal regression (Erhardt et al., 2011).

2.4. Component selection and dynamic FNC estimation

Of the 100 spatial ICA components, we identified 62 components as intrinsic connectivity networks (ICNs) in a semi-automatic manner using the spatial profile of component maps, and dominant low frequency spectral power of their time courses as described in (Allen et al., 2011). The corresponding ICN time courses of each subject were orthogonalized against estimated head movement parameters in a regression framework and then filtered using 5th order Butterworth filter with a passband of 0.01 to 0.15 Hz. Following (Allen et al., 2012a), we performed dynamic functional network connectivity analysis using the post processed ICN time courses. Briefly, we computed pairwise correlations between tapered windowed segments (a rectangular window of 30 TR (60s) convolved with a Gaussian kernel of $\sigma = 3s$) of time courses sliding in steps of 1 TR. This resulted in 1500–30=1470 windows over which we estimated dFNC between 62 independent network time courses (1891 pairs). Since the number of samples are smaller than a static approach using all the timecoure information, we used a robust estimation strategy employing the graphical LASSO method (Friedman et al., 2008) by placing a penalty on the L1 norm of the precision matrix (inverse correlation matrix) to promote sparsity. Given the concerns with estimation of dFNC using shorter windows (Leonardi and Van De Ville, 2015; Lindquist et al., 2014; Smith et al., 2011), we repeated the analysis with longer tapered window sizes of size 45 TR, 60 TR, and shorter tapered window sizes of size 16 TR and 22 TR.

2.5. K-means clustering and comparison to EEG hypnogram

The dFNC windows from a given sliding window were clustered using the K-means algorithm in two steps consistent with our previous work (Allen et al., 2012a). We first

computed a time course of standard deviation of dFNC matrices for each subject and selected subset of subject windows corresponding to local maxima in standard deviation as subject exemplars. These subset exemplars were clustered using K-means algorithm with Manhattan (L1) distance as distance measure. The number of clusters was set to 5 based on elbow criterion of ratio of within to between cluster distance of windows from cluster centroids, referred to as dFNC states. The obtained centroids were used as starting points to cluster all the data. This two step procedure, one to identify initial starting points and subsequent clustering of all window data using these starting points results in stable centroid patterns across independent datasets. The K-means clustering (a hard clustering approach) assigns each dFNC window to one of the dFNC states. This assignment of subject windows in time to dFNC states results in a discrete vector referred to as state vector. Figure 1 shows the schematic of the analysis pipeline used in the paper. We assessed the correspondence between subject dFNC state vector and EEG-derived hypnogram using correlation. To further visualize the correspondence between dFNC estimates from the sliding-window method and EEG-based subject hypnogram, we project the multidimensional (1891) dFNC data into 2 dimensions using the t-distributed stochastic neighborhood embedding (t-SNE) algorithm that preserves the distances between similar objects in high dimensional space to low dimensions (van der Maaten et al., 2008). We also sought to characterize the temporal properties of state vectors obtained from each modality by computing state transition probabilities from these vectors and then compare the similarities between the two vectors.

In our earlier work (Allen et al., 2017), we aligned FNC state vectors to EEG using the time point corresponding to the center of the sliding window. As that study was performed during awake conditions only (eyes open and eyes closed awake conditions), we did not have many EEG-based transitions within the subject wakeful state. Since the data from this study has a ground truth (EEG-based) hypnogram transition state vector informing of subject's sleep stage, we performed a classification study using linear support vector machine (SVM) to see if the alignment of EEG hypnogram best corresponds to start or middle or in-between shift (3, 5 or 7 TRs) of dFNC state vector obtained from sliding window size of 30s. Prior to running SVM, the dFNC connectivity matrix (1891 pairs) was reduced to 30 dimensions using PCA. An 11 fold cross-validation was performed to assess the consistency of best alignment. For each fold, 5 different subjects were left out and a linear SVM was trained on remaining 50 subjects using libsvm package (https://www.csie.ntu.edu.tw/cjlin/libsvm/). A multi-class (all pairs/one-against-one) linear SVM model identifies support points in kernel space that maximally separates each pair of classes (W-N1,W-N2,W-N3,N1-N2,N1-N3,N2-N3). Then each test case/window is assigned to the class that gets most votes. Both training and test balanced (averaged per class) accuracies were computed. The two awake dFNC states were collapsed into one for this analysis. The analysis was repeated with radial basis function (RBF) kernel. For linear SVM, the optimum penalty parameter C was identified using grid search between [0.1 and 10]. For RBF SVM, the a grid search was performed to identify optimal hyperparameters C and gamma in the range [0.1 to 10] and [1e-03 to 1e-01] respectively.

To identify optimal window size among the tested window sizes, we performed another linear SVM separately for dFNC windows obtained with each choice of window length. Similar cross-validation analysis as mentioned above was used. Finally, we also tested the

performance of the DCC algorithm, which uses adaptive windowing, to track subject sleep state. The DCC algorithm fits univariate generalized autoregressive conditional heteroscedastic (GARCH) GARCH(1,1) models to each univariate time series to obtain standardized residuals and then applies an exponentially weighted moving average window on these standard residuals of each pair of time courses to compute a non-normalized version of time-varying correlation between the two time courses (see (Lindquist et al., 2014; Choe et al., 2017) for more details).

To investigate if wakeful state can be further clustered into meaningful sub-clusters as in our earlier work, we restricted our clustering analysis to the 26001 dFNC windows (State 1 for window size 30) that corresponded to the subject wakeful EEG condition. This analysis revealed 4 sub-clusters with distinct connectivity profiles. We ran a SVM classification analysis by holding out 6000 dFNC windows and performed a three fold cross validation on the remaining 20000 windows to estimate a model for a RBF kernel. The best model was then used to test the classification accuracy on the held out samples and we computed average per class accuracy and confusion matrix.

2.6. Head motion effects

To assess the impact of subject head motion on the connectivity estimates, we assessed the relationship between the subject head movement summaries and dFNC state vector. We computed framewise displacement (FD) and framewise data variation (DVARS) (Power et al., 2012) for each subject to represent their motion summary. We then computed the number of instances subject DVARS exceeds its mean by 2.5 times its standard deviation for each k-means state. A one-way ANOVA was then performed on the counts to see if certain states show significantly more motion related outliers. In addition, we plotted each subject state vector along with their FD and DVARS to visually assess if any of the states are contaminated by head movement.

3. Results

The sixty-two ICNs selected for subsequent analysis are depicted in Figure 2. These components are grouped into subcortical (5), auditory (2), sensorimotor (10), visual (11), a set of higher order associative areas involved in attentional and executive control as well as cognitive control (19), default-mode regions (10) and cerebellar (5) components based on anatomical proximity and functional connectivity as in our earlier studies (Allen et al., 2012a, 2011). The selected 62 ICN labels are summarized in Table 1.

3.1. dFNC clustering results

The centroids (k=5) obtained from k-means clustering of dynamic FNC window data of all subjects are shown in Figure 3A. The centroids were ordered according to their frequency of occurrence in time (from the most awake state to the deepest sleep state), with the exception of state 2 Figure 3B. These centroids show distinct connectivity patterns from state to state. Estimation of modularity of the centroid states using the Louvain community detection algorithm (Rubinov and Sporns, 2011) resulted in three modules for states 1,2 and 3, and four modules for states 4 and 5. Although subcortical and cerebellar ICs belong to the same

module in all states, they segregate as an additional module for states 4 and 5. We computed mean within module connectivity strength and the top 12 ICs for each module are shown in Figure 3C.

3.2. Do clustered connectivity states correspond to sleep states?

The subject-state vectors are sorted by sleep state (W, N1, N2 and N3) and frequency counts by sleep state were obtained and are shown in Figure 4. As seen in the figure, connectivity patterns in states 1 and 2 predominantly occur in the awake state while the patterns seen in states 3, 4 and 5 occur more frequently as subjects fall into different sleep states gradually with the connectivity pattern in state 5 occurring during N3 (deep) sleep stage.

We tested the correspondence between subject state vectors obtained through clustering dFNC matrices and subject hypnograms obtained by computing the cross-correlation between the two vectors. Figure 5 shows examples of subjects with the two best and the two worst correlations between the two. As seen in the figure, the best subject showed a correlation of 0.89 between his/her hypnogram and state vector. The subjects that showed the poorest correlation between the two primarily tended to stay awake throughout the scan session, and the dFNC state vector showed transitions between awake related states 1 and 2.

The results assessing the correspondence between subject dFNC state vector and his/her hypnogram are summarized in Figure 6. For this projection, a random sample of 400 dFNC windows by state (total 2000 points) were visualized using the t-SNE algorithm and were color coded with their corresponding k-means cluster assignment (Fig 6A) or by sleep stage obtained from the respective hypnogram (Fig 6B). Both awake states from the k-mean clustering are grouped together and show a transition from wakefulness to deeper sleep stages that occurs gradually along a smooth trajectory. This result shows that the dFNC estimates using the sliding window method and subsequent clustering correspond well to neurophysiological states as estimated via the EEG-based hypnogram.

3.3. How does motion affect the clustering?

To assess the effect of subject head movement during the scan on dFNC clustering results, we computed the number of windows with significant subject head movements (points greater that 2.5 standard deviations from mean framewise displacement) for each dFNC state and also visually assessed subject dFNC state vector and mean framewise displacement vectors. State 2 is associated with larger head movements during the scan relative to the other states. The number of significant head movements by state are shown in Supplemental Figure S1A. A couple of example subject state vectors and their head movement summary (FD) vectors are also shown in Supplemental Figure S1B.

3.4. Characterization of temporal dynamics

Comparison of the temporal properties of state vectors obtained from each modality is summarized in (Figure 7). The average dwell times and frequency of occurrence of each state are consistent for data from both modalities. The state transition matrices show good correspondence with more probable transitions from W->N1, N1->N2, N2->N3 and transitions to the W state from all sleep stages. This is in line with our knowledge of

progression into various sleep stages. However, we observe a higher average number of transitions between states from the dFNC clustering derived state vectors compared to those computed using the EEG derived hypnogram.

3.5. Alignment of EEG derived hypnogram and windowed dFNC data

The SVM classification results for best alignment of EEG hypnogram and dFNC window position are presented in Figure 8. The results suggest that maximum accuracy is obtained when dFNC state vector is aligned to corresponding EEG hypnogram vector by the starting point of the window and the classification performance is reduced when a shift is introduced between the two vectors.

3.6. How well can we predict sleep stages from dFNC data?

The SVM classification accuracies comparing the prediction of subject hypnogram with dFNC estimates obtained using different window lengths is presented in Figure 9. As seen in the figure, the classification accuracy significantly increases with dFNC estimates from shorter to longer window sizes in training subject cases (the data SVM model has seen: one-way ANOVA $F=342, p<1e-35$). The accuracies on left out test samples did not significantly differ with window sizes (one-way ANOVA $F=0.7, p>0.58$). These accuracy rates are consistent with earlier reports (Tagliazucchi et al., 2012b) however we show that these can be achieved using much shorter window lengths. The classification accuracies for dFNC estimates using DCC method performed poorly compared to those obtained using sliding window methods for all window sizes.

3.7. Does wakeful stage correspond to only one dFNC cluster?

Since our prior work (Allen et al., 2017) showed multiple wakeful states with distinct EEG spectral signatures, we further focused on the awake condition only to see if it can be reliably segmented into sub-clusters. A search for the optimal number of clusters using the elbow criterion yielded four clusters. The cluster centroids are depicted in Figure 10. Awake state cluster centroids 1 and 2 resemble each other but differ in the strength of correlations in within and between module groupings. Awake state 4 resembles state 3 from the full dataset but distinguishes itself in anti-correlations between sensory (visual, motor and auditory) networks to higher order cognitive networks and also to the default-mode regions. Results from SVM classification of awake only cluster windows resulted in 92% classification accuracy using a one-vs-rest RBF SVM model with grid search. The resulting confusion matrix is presented in Table 2. The classification is performed using leave 10% subjects out in a five fold cross-validation scheme. Classification accuracy reaches chance level of 25% when the class labels are permuted. This result suggests that the sub-clusters obtained from awake state are linearly separable with high accuracy.

4. Discussion

In this work, using an ICA based pipeline, we assess the ability of sliding window correlation based dynamic functional network connectivity measures to capture neurophysiological state transitions obtained from sleep staging of EEG data that was concurrently acquired during resting fMRI acquisition. Results show a good correspondence

between the subject state vectors obtained from k-means clustering of dFNC windows and subject hypnograms. We further demonstrate that distinct resting functional connectivity patterns are associated with wakeful and sleep states with dFNC state 1 predominantly occurring while subjects are awake, dFNC state 3 corresponding to reduced subject vigilance and early sleep stage (N1) and dFNC states 4 and 5 are more likely to be associated with deeper sleep stages. Deep sleep (N3) is primarily associated with dFNC state 5 across all subjects. One state (dFNC state 2) primarily captures variance associated with subject movement.

4.1. dFNC clustering estimates can reliably predict subject sleep state

Recently, using the same data reported in this work, Haimovici et al. (2017) showed good correspondence between centroids of windowed resting fMRI correlation data obtained from k-means clustering and those informed by an EEG-based hypnogram. In Haimovici et al. (2017), the connectivity measures were estimated from non-overlapping windows of length 100 seconds within fixed regions of interest and so precludes time varying connectivity information. Our work replicated the aforementioned result in Haimovici et al. (2017) despite several differences including the use of time-varying connectivity estimates from ICA derived network time courses as well as the use of overlapping windows with a step size of 1 TR. Using this approach, we show that high classification accuracies can be obtained for windows as short as 30 seconds (15 TRs).

Our results also demonstrated that dFNC estimates from sliding window correlation show higher accuracy compared to an adaptive windowless dynamic conditional correlation method. However, DCC estimates from sliding window based covariance estimates resulted in classification accuracies similar to those obtained from the sliding window method suggesting this parametric model of conditional correlation for resting fMRI data might be more sensitive to noise than smoother sliding window estimates when instantaneous conditional correlation estimates are computed.

Our analysis demonstrates that even window lengths as short as 30 seconds result in reasonable estimates of time-varying connectivity profiles with estimated dFNC clustering states showing good classification accuracy with subject hypnogram. This is in line with previous reports (Shirer et al., 2012) and suggests that the $1/f_{min}$ recommendation for window length as recommended by Leonardi and Van De Ville (2015) might be too conservative (Vergara and Calhoun, 2018). In our case $1/f_{min}$ would result in 100 sec (since f_{min} = 0.01 Hz after filtering) and may limit our ability to capture dynamics for $1/f$ spectral distributed BOLD data (Zalesky and Breakspear, 2015).

The observed differences between the individual dFNC state vector and the hypnogram can arise for the following reasons. The hypnogram is scored from EEG data epochs of 30 seconds and assigns each 30 second segment to a single hypnogram stage (W/N1/N2 or N3). The dFNC at a given instant is estimated from a window length ‘w’ on either side of the time point (past and future). However, k-means is a hard clustering approach and, as seen in Figure 6, there is ambiguity in the assignment of the data point with its immediate neighboring state (for example dFNC states 4 and 5 and corresponding N2 and N3 sleep stages) compared to the ground truth (hypnogram). Fuzzy k-means approaches can help

mitigate this issue by allowing for states to overlap with one another (Miller et al., 2016). Another source of possible differences may be due to the different impact of noise (e.g. motion, MRI gradients) on the two signals which can hinder our ability of accurately estimating subject states.

4.2. Head motion appears to be separable from dynamic connectivity measures

Our dFNC clustering analysis reveals that motion appears to be mostly associated with one of the states (dFNC state 2) rather than spread across all of them. An examination of classification errors by sleep stage obtained for a window length of 30 TRs suggested that the awake state has the least errors (about 10%) and N1 sleep stage had the most errors (approximately 40%), with deeper sleep stages having an error rate of about 20%. Further evaluation to determine if dFNC windows overlapping with larger head movements during the scan drive these errors suggested that motion only contributed to about 15% of misclassified cases evenly across wakeful and sleep stages i.e 15% of 10, 40, 20 and 20 error rates of W, N1, N2, and N3 stages respectively. This suggests that dFNC windows exhibit larger variability during the N1 sleep stage compared to other sleep stages as observed in Supplemental Figure S2 leading to misclassification. This highlights the need to further identify additional sub-clusters in the N1 sleep stage and investigate if a fine grained EEG classification of this stage as proposed by Hori and colleagues (Hori et al., 1994) and recently demonstrated using EEG data (Jagannathan et al., 2018) can provide additional insights into large scale connectivity changes during the transition to sleep (Goupil and Bekinschtein, 2012).

4.3. Evidence of multiple dFNC sub-clusters states during wakefulness

The elbow criterion, computed as a ratio of between-cluster to within-cluster distance, was used to obtain an optimal k for clustering of the data using the k-means algorithm. Results suggest a 5 cluster solution within which we observe fewer (two) states from the wakeful portions of the scans than those reported earlier for data collected during the wakeful condition only (Allen et al., 2012b, 2017). This could be due to the fact that variability in dFNC fluctuations during wakefulness is lower compared to variability across different sleep stages (see Supplemental Figure S2). To evaluate this further, we performed a separate elbow criterion search and clustering of dFNC windows within only the wakeful state to see if additional clusters of meaningful time-varying connectivity profiles within and across subjects can be reliably estimated. Separate K-means clustering of dFNC windows from the awake only state (state 1) revealed additional sub-clusters not seen from clustering the data including all sleep stages. Windows corresponding to these sub-clusters are linearly separable with good accuracy using a linear SVM classifier. This result is in line with and extends recent reports showing replicable dFNC states in multiple independent datasets (Abrol et al., 2017) during (unconfirmed) wakeful conditions.

Some recent studies have argued that the observed connectivity states during wakefulness are primarily a reflection of sampling variability, changes in subject vigilance and partly reflect changes due to head movement (Laumann et al., 2016; Liegeois et al., 2017; Haimovici et al., 2017). Spontaneous eye blinks during wakefulness have also been shown to cause connectivity fluctuations in resting fMRI data (Wang et al., 2016). Another view is

that time-varying connectivity changes in resting state fMRI can be modeled as hierarchical transitions between connectivity states consisting of two metastates: one corresponding to states with increased connectivity in brain regions involved in higher cognition and other corresponding to states with greater integration within sensory regions (Vidaurre et al., 2017). Another recent study identified strong correlation between dFC obtained using sliding window correlation of BOLD data and temporal dynamics of calcium signal during rest in mice brain recordings suggesting a neuronal origin of the observed dynamics (Matsui et al., 2018). In this work, we show distinct connectivity states during wakefulness that are separable via a cross-validated linear classifier. Future studies should evaluate the underlying neurobiological signatures of both sleep and wakefulness in greater detail. Transition between wakefulness to light sleep (N1) is associated with increased cortico-cortical connectivity and reduced sub-cortical cortical connectivity. N1 to N2 sleep transition is reduction in between and within sensory domain connectivity and increased connectivity between cerebellar ICNs. Finally deep sleep (N3) is associated with further reductions in long range connectivity between ICNs resulting in connectivity patterns closer to structural connectivity consistent with earlier reports.

4.4. Limitations and future work

We did not compare the sliding window correlation method to alternative methods of dynamic connectivity methods like multiplication of temporal derivatives (Shine et al., 2015) and time-frequency approaches (Yaesoubi et al., 2015c). The current dFNC patterns reported only correspond to certain sleep stages observed during the one hour scan performed early in the night. Further studies are needed to fully characterize functional connectivity during other known sleep states like rapid eye movement (REM) sleep possibly by scanning late in the night or from early morning recordings. Also, in this work we show the presence of linearly separable (predictable) connectivity states during wakeful rest to extend our previous work and address some current technical controversies in the field. Going forward, it would be interesting to perform a hierarchical analysis of various sleep stages to evaluate the possibility of different states existing during different sleep stages as well as to further study the underlying neurobiological correlates of these states with the use of multimodal imaging data along with novel modeling techniques.

4.5. Conclusions

In this work, using an ICA-based pipeline applied to concurrent EEG/fMRI data collected during wakefulness and various sleep stages we demonstrate that time varying connectivity estimates from sliding windowed correlations of resting state functional network time courses well classify the sleep states obtained from EEG data even for windows as short as 30 seconds. We show that head motion is mostly associated with one of the states rather than spread across all of them. Consistent with earlier work, we find increased variability in connectivity as subjects transition from wakefulness to sleep. We report linearly separable clusters within the wakeful state and suggest future directions for assessing their neurobiological relevance via hierarchical analysis of predictable states in various sleep stages measured with EEG-fMRI data including eye tracking during the wakeful condition.

Supplementary Material

Refer to Web version on PubMed Central for supplementary material.

Acknowledgements

This work was funded by NIH P20GM103472, Ro1EB006841 and NSF EPSCoR 1539067 and the Bundesministerium für Bildung und Forschung (grant 01 EV 0703) and the LOEWE Neuronale Koordination Forschungsschwerpunkt Frankfurt (NeFF).

Bibliography

AASM, Iber C, 2007 The AASM Manual for the Scoring of Sleep and Associated Events: Rules, Terminology and Technical Specifications. American Academy of Sleep Medicine.

Abrol A, Damaraju E, Miller RL, Stephen JM, Claus ED, Mayer AR, Calhoun VD, 2017 Replicability of time-varying connectivity patterns in large resting state fMRI samples. Neuroimage 163, 160–176. [PubMed: 28916181]

Allen EA, Damaraju E, Eichele T, Wu L, Calhoun VD, 2017 EEG Signatures of Dynamic Functional Network Connectivity States. Brain Topography, 1–16. [PubMed: 27796603]

Allen EA, Damaraju E, Plis SM, Erhardt EB, Eichele T, Calhoun VD, 2012a Tracking Whole-Brain Connectivity Dynamics in the Resting State. Cerebral Cortex. URL http://cercor.oxfordjournals.org/content/early/2012/11/09/cercor.bhs352.abstract

Allen EA, Erhardt EB, Damaraju E, Gruner W, Segall JM, Silva RF, Havlicek M, Rachakonda S, Fries J, Kalyanam R, Michael AM, Caprihan A. a. Turner J, Eichele T, Adelsheim S, Bryan AD, Bustillo J, Clark VP, Feldstein Ewing SW, Filbey F, Ford CC, Hutchison K, Jung RE, a. Kiehl K, Kodituwakku P, Komesu YM, Mayer AR, Pearlson GD, Phillips JP, Sadek JR, Stevens M, Teuscher U, Thoma RJ, Calhoun VD, 2011 A Baseline for the Multivariate Comparison of Resting-State Networks. Frontiers in systems neuroscience 5, 2 URL http://www.pubmedcentral.nih.gov/articlerender.fcgi?artid=3051178{&}tool=pmcentrez{&}rendertype=abstract [PubMed: 21442040]

Allen EA, Erhardt EB, Wei Y, Eichele T, Calhoun VD, 2012b Capturing Inter-Subject Variability With Group Independent Component Analysis of fMRI Data: a Simulation Study. NeuroImage 59 (4), 4141–59. URL 10.1016/j.neuroimage.2011.10.010 [PubMed: 22019879]

Allen PJ, Polizzi G, Krakow K, Fish DR, Lemieux L, 1998 Identification of EEG Events in the MR Scanner: the Problem of Pulse Artifact and a Method for Its Subtraction. NeuroImage 8 (3), 229–239. [PubMed: 9758737]

Barttfeld P, Uhrig L, Sitt JD, Sigman M, Jarraya B, Dehaene S, 2015 Signature of consciousness in the dynamics of resting-state brain activity. Proceedings of the National Academy of Sciences 112 (3), 887–892.

Calhoun VD, Adali T, 2012 Multisubject Independent Component Analysis of fMRI: a Decade of Intrinsic Networks, Default Mode, and Neurodiagnostic Discovery. Biomedical Engineering, IEEE Reviews in 5, 60–73.

Calhoun VD, Adali T, Pearlson GD, Pekar JJ, 2001 A Method for Making Group Inferences From Functional MRI Data Using Independent Component Analysis. Human Brain Mapping 14 (3), 140–51. URL http://www.ncbi.nlm.nih.gov/pubmed/11559959 [PubMed: 11559959]

Calhoun VD, de Lacy N, 2017 Ten key observations on the analysis of resting-state functional mr imaging data using independent component analysis. Neuroimaging Clinics 27 (4), 561–579. [PubMed: 28985929]

Calhoun VD, Kiehl KA, Pearlson GD, 2008 Modulation of Temporally Coherent Brain Networks Estimated Using ICA at Rest and During Cognitive Tasks. Human Brain Mapping 29 (7), 828–838. [PubMed: 18438867]

Calhoun VD, Miller R, Pearlson G, Adali T, 2014 The Chronnectome: Time-Varying Connectivity Networks As the Next Frontier in fMRI Data Discovery. Neuron 84 (2), 262–274. [PubMed: 25374354]

Chang C, Glover GH, 2010 Time-Frequency Dynamics of Resting-State Brain Connectivity Measured With fMRI. NeuroImage 50 (1), 81–98. URL http://www.pubmedcentral.nih.gov/articlerender.fcgi?artid=2827259{&}tool=pmcentrez{&}rendertype=abstract [PubMed: 20006716]

Chang C, Leopold DA, Schölvinck ML, Mandelkow H, Picchioni D, Liu X, Frank QY, Turchi JN, Duyn JH, 2016 Tracking Brain Arousal Fluctuations With fMRI. Proceedings of the National Academy of Sciences, 201520613.

Choe AS, Nebel MB, Barber AD, Cohen JR, Xu Y, Pekar JJ, Caffo B, Lindquist MA, 2017 Comparing test-retest reliability of dynamic functional connectivity methods. NeuroImage.

Cribben I, Wager T, Lindquist M, 2013 Detecting functional connectivity change points for single-subject fMRI data. Frontiers in computational neuroscience 7, 143. [PubMed: 24198781]

Damaraju E, Allen EA, Belger A, Ford JM, McEwen S, Mathalon DH, Mueller BA, Pearlson GD, Potkin SG, Preda A, 2014 Dynamic Functional Connectivity Analysis Reveals Transient States of Dysconnectivity in Schizophrenia. NeuroImage: Clinical 5, 298–308. [PubMed: 25161896]

Engle R, 2002 Dynamic conditional correlation: A simple class of multivariate generalized autoregressive conditional heteroskedasticity models. Journal of Business & Economic Statistics 20 (3), 339–350.

Erhardt EB, Rachakonda S, Bedrick EJ, Allen EA, Adali T, Calhoun VD, 2011 Comparison of Multi-Subject ICA Methods for Analysis of fMRI Data. Human Brain Mapping 32 (12), 2075–2095. URL 10.1002/hbm.21170 [PubMed: 21162045]

Friedman J, Hastie T, Tibshirani R, 2008 Sparse Inverse Covariance Estimation With the Graphical Lasso. Biostatistics 9 (3), 432–441. URL http://biostatistics.oxfordjournals.org/content/9/3/432.abstract [PubMed: 18079126]

Goupil L, Bekinschtein T, 2012 Cognitive processing during the transition to sleep. Archives italiennes de biologie 150 (2/3), 140–154. [PubMed: 23165874]

Haimovici A, Tagliazucchi E, Balenzuela P, Laufs H, 2017 On wakefulness fluctuations as a source of BOLD functional connectivity dynamics. Scientific Reports 7.

Himberg J, Hyvärinen A, Esposito F, 2004 Validating the Independent Components of Neuroimaging Time Series Via Clustering and Visualization. NeuroImage 22 (3), 1214–1222. [PubMed: 15219593]

Hindriks R, Adhikari MH, Murayama Y, Ganzetti M, Mantini D, Logothetis NK, Deco G, 2016 Can sliding-window correlations reveal dynamic functional connectivity in resting-state fmri? Neuroimage 127, 242–256. [PubMed: 26631813]

Hori T, Hayashi M, Morikawa T, 1994 Topographical EEG changes and the hypnagogic experience.

Hutchison RM, Womelsdorf T, Allen EA, Bandettini PA, Calhoun VD, Corbetta M, Penna SD, Duyn J, Glover G, Gonzalez-Castillo J, 2013 Dynamic Functional Connectivity: Promises, Issues, and Interpretations. NeuroImage.

Jagannathan SR, Ezquerro-Nassar A, Jachs B, Pustovaya OV, Bareham CA, Bekinschtein TA, 2018 Tracking wakefulness as it fades: Micro-measures of alertness. NeuroImage 176, 138–151. URL http://www.sciencedirect.com/science/article/pii/S1053811918303562 [PubMed: 29698731]

Kang J, Wang L, Yan C, Wang J, Liang X, He Y, 2011 Characterizing dynamic functional connectivity in the resting brain using variable parameter regression and kalman filtering approaches. Neuroimage 56 (3), 1222–1234. [PubMed: 21420500]

Laumann TO, Snyder AZ, Mitra A, Gordon EM, Gratton C, Adeyemo B, Gilmore AW, Nelson SM, Berg JJ, Greene DJ, McCarthy JE, Tagliazucchi E, Laufs H, Schlaggar BL, Dosenbach NUF, Petersen SE, 2016 On the Stability of BOLD fMRI Correlations. Cerebral Cortex. URL http://cercor.oxfordjournals.org/content/early/2016/09/01/cercor.bhw265. abstract

Leonardi N, Van De Ville D, 2015 On Spurious and Real Fluctuations of Dynamic Functional Connectivity During Rest. NeuroImage 104, 430–436. [PubMed: 25234118]

Liegeois R, Laumann TO, Snyder AZ, Zhou J, Yeo BT, 2017 Interpreting temporal fluctuations in resting-state functional connectivity MRI. Neuroimage.

Lindquist MA, Xu Y, Nebel MB, Caffo BS, 2014 Evaluating Dynamic Bivariate Correlations in Resting-State fMRI: a Comparison Study and a New Approach. NeuroImage 101, 531–46. URL http://www.sciencedirect.com/science/article/pii/S1053811914005291 [PubMed: 24993894]

Matsui T, Murakami T, Ohki K, 2018 Neuronal origin of the temporal dynamics of spontaneous bold activity correlation. Cerebral Cortex. URL 10.1093/cercor/bhy045

Miller RL, Yaesoubi M, Turner JA, Mathalon D, Preda A, Pearlson G, Adali T, Calhoun VD, 2016 Higher dimensional meta-state analysis reveals reduced resting fMRI connectivity dynamism in schizophrenia patients. PloS one 11 (3), e0149849. [PubMed: 26981625]

Power JD, Barnes KA, Snyder AZ, Schlaggar BL, Petersen SE, 2012 Spurious But Systematic Correlations in Functional Connectivity MRI Networks Arise From Subject Motion. NeuroImage 59 (3), 2142–54. URL 10.1016/j.neuroimage.2011.10.018 [PubMed: 22019881]

Preti MG, Bolton TA, Van De Ville D, 2017 The dynamic functional connectome: state-of-the-art and perspectives. Neuroimage 160, 41–54. [PubMed: 28034766]

Rubinov M, Sporns O, 2011 Weight-Conserving Characterization of Complex Functional Brain Networks. NeuroImage 56 (4), 2068–2079. [PubMed: 21459148]

Sakoğlu U, Pearlson GD, Kiehl KA, Wang YM, Michael AM, Calhoun VD, 2010 A method for evaluating dynamic functional network connectivity and task-modulation: Application to schizophrenia. Magnetic Resonance Materials in Physics, Biology and Medicine 23 (5–6), 351–366.

Shakil S, Lee C-H, Keilholz SD, 2016 Evaluation of Sliding Window Correlation Performance for Characterizing Dynamic Functional Connectivity and Brain States. NeuroImage 133, 111–128. [PubMed: 26952197]

Shine JM, Oluwasanmi K, Bell PT, Gorgolewski KJ, Gilat M, Poldrack RA, 2015 Estimation of Dynamic Functional Connectivity Using Multiplicative Analytical Coupling. NeuroImage 122, 399–407. URL http://www.sciencedirect.com/science/article/pii/S1053811915006849 [PubMed: 26231247]

Shirer WR, Ryali S, Rykhlevskaia E, Menon V, Greicius MD, 2012 Decoding Subject-Driven Cognitive States With Whole-Brain Connectivity Patterns. Cerebral Cortex 22 (1), 158–165. [PubMed: 21616982]

Smith SM, Fox PT, Miller KL, Glahn DC, Fox PM, Mackay CE, Filippini N, Watkins KE, Toro R, Laird AR, Beckmann CF, 2009 Correspondence of the Brain's Functional Architecture During Activation and Rest. Proceedings of the National Academy of Sciences 106 (31), 13040–5. URL http://www.pnas.org/cgi/content/abstract/106/31/13040

Smith SM, Miller KL, Salimi-Khorshidi G, Webster M, Beckmann CF, Nichols TE, Ramsey JD, Woolrich MW, 2011 Network Modelling Methods for fMRI. NeuroImage 54 (2), 875–891. [PubMed: 20817103]

Tagliazucchi E, Balenzuela P, Fraiman D, Chialvo DR, 2012a Criticality in large-scale brain fMRI dynamics unveiled by a novel point process analysis. Frontiers in physiology 3, 15. [PubMed: 22347863]

Tagliazucchi E, Laufs H, 2014 Decoding Wakefulness Levels From Typical fMRI Resting-State Data Reveals Reliable Drifts Between Wakefulness and Sleep. Neuron 82 (3), 695–708. URL http://www.sciencedirect.com/science/article/pii/S0896627314002505 [PubMed: 24811386]

Tagliazucchi E, von Wegner F, Morzelewski A, Borisov S, Jahnke K, Laufs H, 2012b Automatic sleep staging using fMRI functional connectivity data. NeuroImage 63 (1), 63–72. URL http://www.sciencedirect.com/science/article/pii/S1053811912006507 [PubMed: 22743197]

Tagliazucchi E, von Wegner F, Morzelewski A, Brodbeck V, Jahnke K, Laufs H, 2013 Breakdown of Long-Range Temporal Dependence in Default Mode and Attention Networks During Deep Sleep. Proceedings of the National Academy of Sciences 110 (38), 15419–15424.

van der Maaten Laurens, Hinton Geoffrey, 2008 Visualizing data using t-SNE. The Journal of Machine Learning Research 9 (2579–2605), 85.

Vergara V, Calhoun VD, 2018 Which dFNC Window Length is Valid? In: Organization of Human Brain Mapping Singapore.

Vidaurre D, Smith SM, Woolrich MW, 2017 Brain network dynamics are hierarchically organized in time. Proceedings of the National Academy of Sciences 114 (48), 12827–12832. URL http://www.pnas.org/content/114/48/12827

Wang C, Ong JL, Patanaik A, Zhou J, Chee MW, 2016 Spontaneous eyelid closures link vigilance fluctuation with fMRI dynamic connectivity states. Proceedings of the National Academy of Sciences 113 (34), 9653–9658.

Yaesoubi M, Allen EA, Miller RL, Calhoun VD, 2015a Dynamic coherence analysis of resting fMRI data to jointly capture state-based phase, frequency, and time-domain information. NeuroImage 120, 133–142. URL http://www.sciencedirect.com/science/article/pii/S1053811915006096 [PubMed: 26162552]

Yaesoubi M, Miller RL, Calhoun VD, 2015b Mutually Temporally Independent Connectivity Patterns: a New Framework to Study the Dynamics of Brain Connectivity at Rest With Application to Explain Group Difference Based on Gender. NeuroImage 107, 85–94. [PubMed: 25485713]

Yaesoubi M, Miller RL, Calhoun VD, 2015c Mutually temporally independent connectivity patterns: A new framework to study the dynamics of brain connectivity at rest with application to explain group difference based on gender. NeuroImage 107, 85–94. [PubMed: 25485713]

Yu Q, Du Y, Chen J, He H, Sui J, Pearlson G, Calhoun VD, 2017 Comparing brain graphs in which nodes are regions of interest or independent components: A simulation study. Journal of neuroscience methods 291, 61–68. [PubMed: 28807861]

Zalesky A, Breakspear M, 2015 Towards a statistical test for functional connectivity dynamics. NeuroImage 114, 466–470. URL http://www.sciencedirect.com/science/article/pii/S1053811915002293 [PubMed: 25818688]

Zalesky A, Fornito A, Cocchi L, Gollo LL, Breakspear M, 2014 Time-resolved resting-state brain networks. Proceedings of the National Academy of Sciences, 201400181.

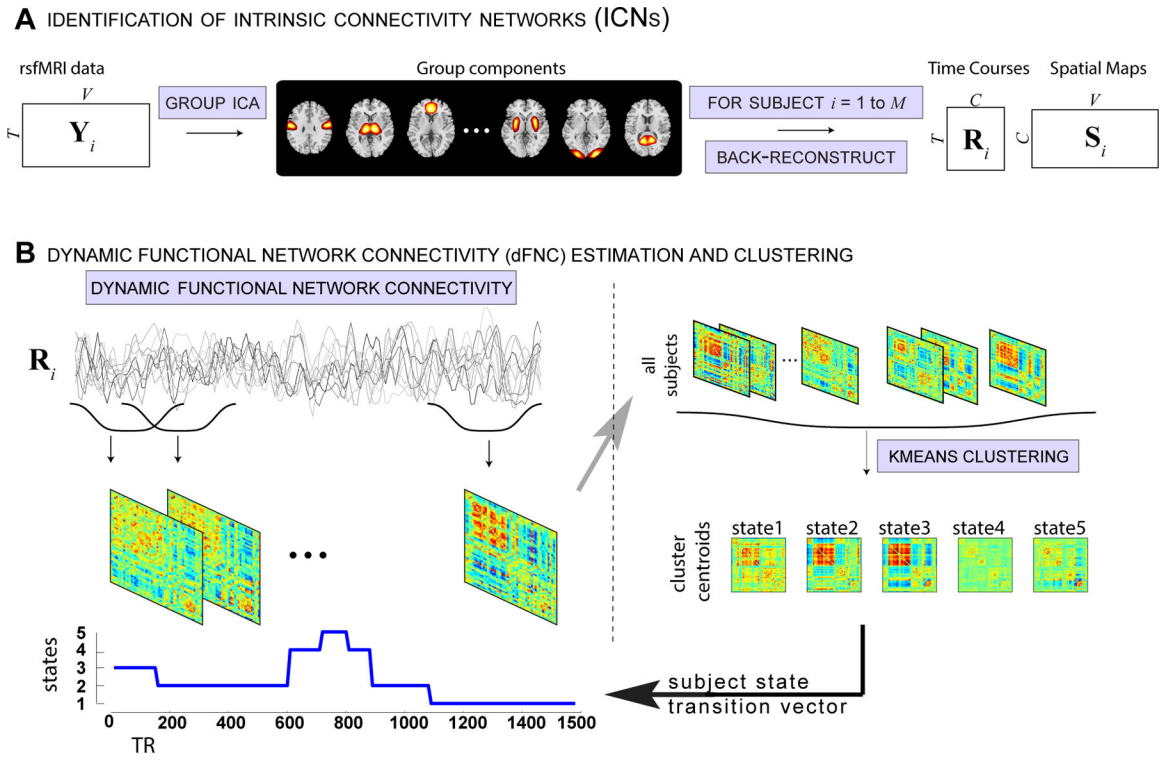

Figure 1:
Schematic depicting resting fMRI data processing (adapted from (Damaraju et al., 2014)).

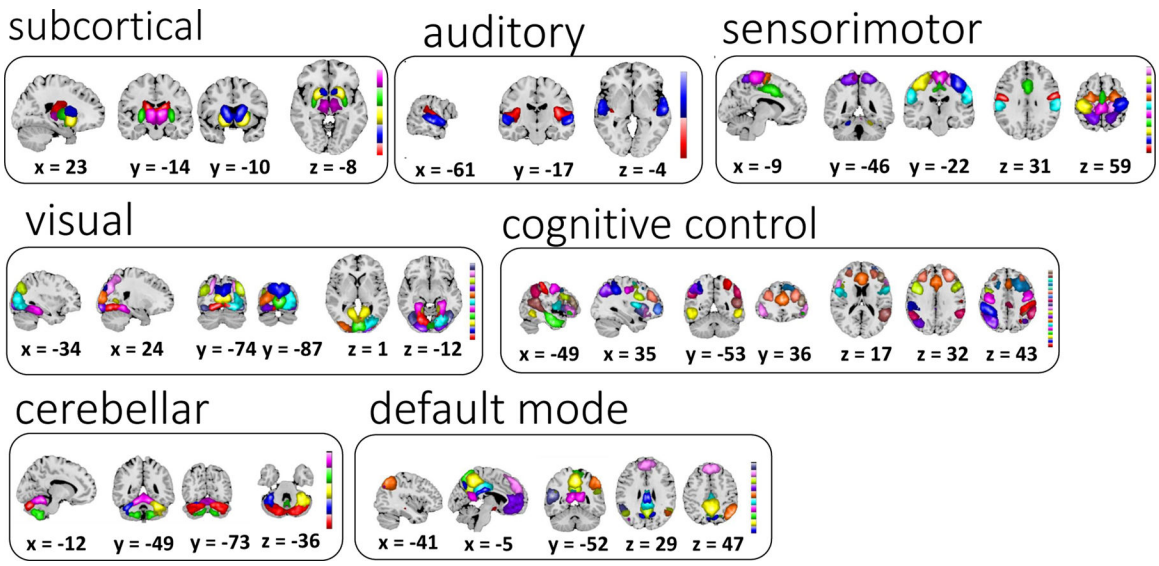

Figure 2:

Sixty-two selected ICNs for further analysis were grouped into 7 modules using previously reported methods (Allen et al., 2012b).

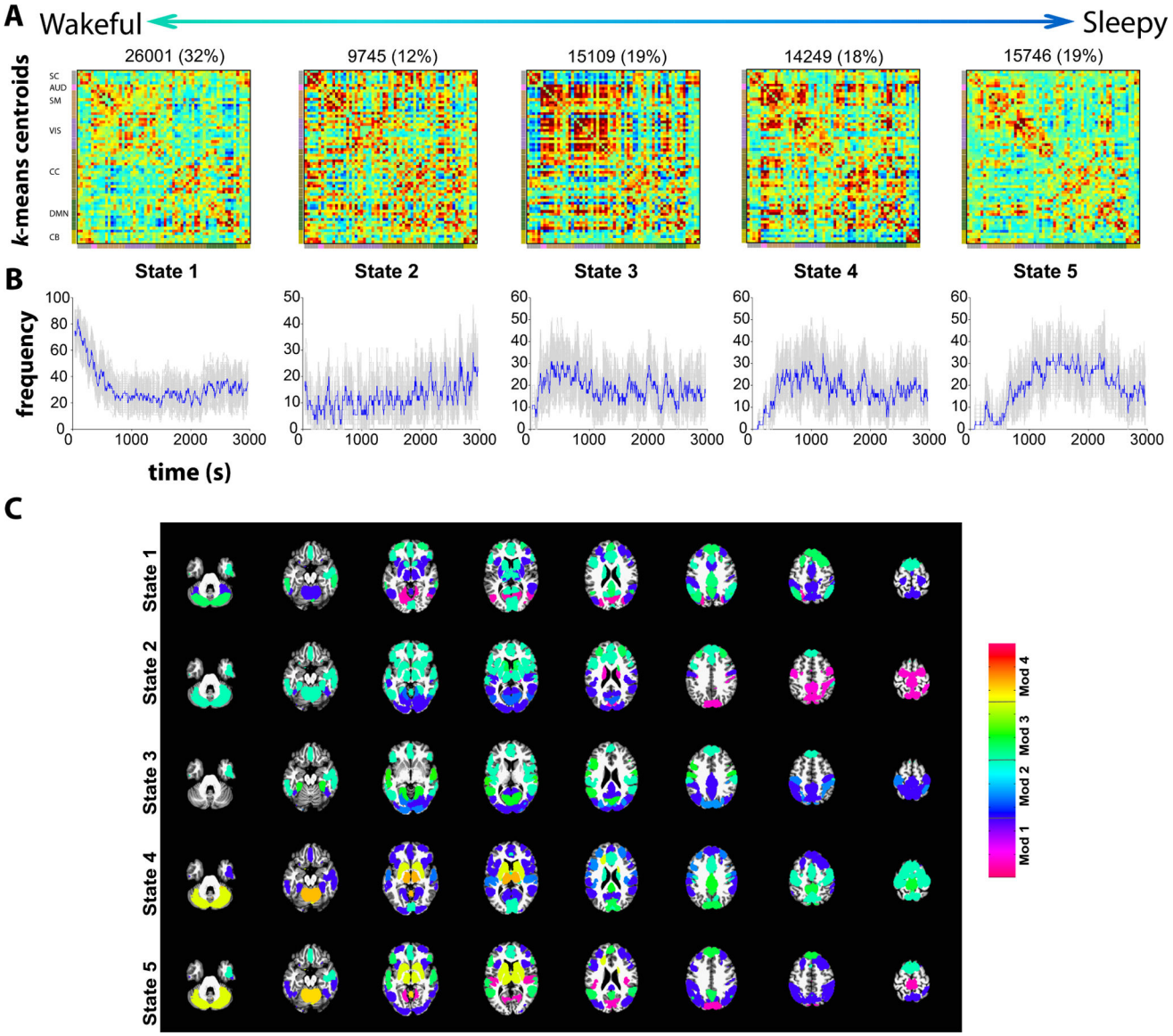

Figure 3:

Cluster centroids from k-means clustering of dFNC window data for window size 30 (A) and the frequency of occurrence of each state in time (B). The standard errors for the frequency of occurrence were computed using 100 bootstrap resamples of the subject dFNC window data. (C) The modularity of the centroids is computed using the Louvain algorithm ("modularity_louvain_und_sign.m" function in the Brain Connectivity toolbox) resulting in three modules (Mod) for states 1,2 and 3 and four modules for states 4 and 5. The top 12 ICs with highest mean within module FC are depicted scaled by mean within module FC. Note that the weights (mean within module connectivity) are lower in states 1 and 5 compared to states 2, 3 and 4.

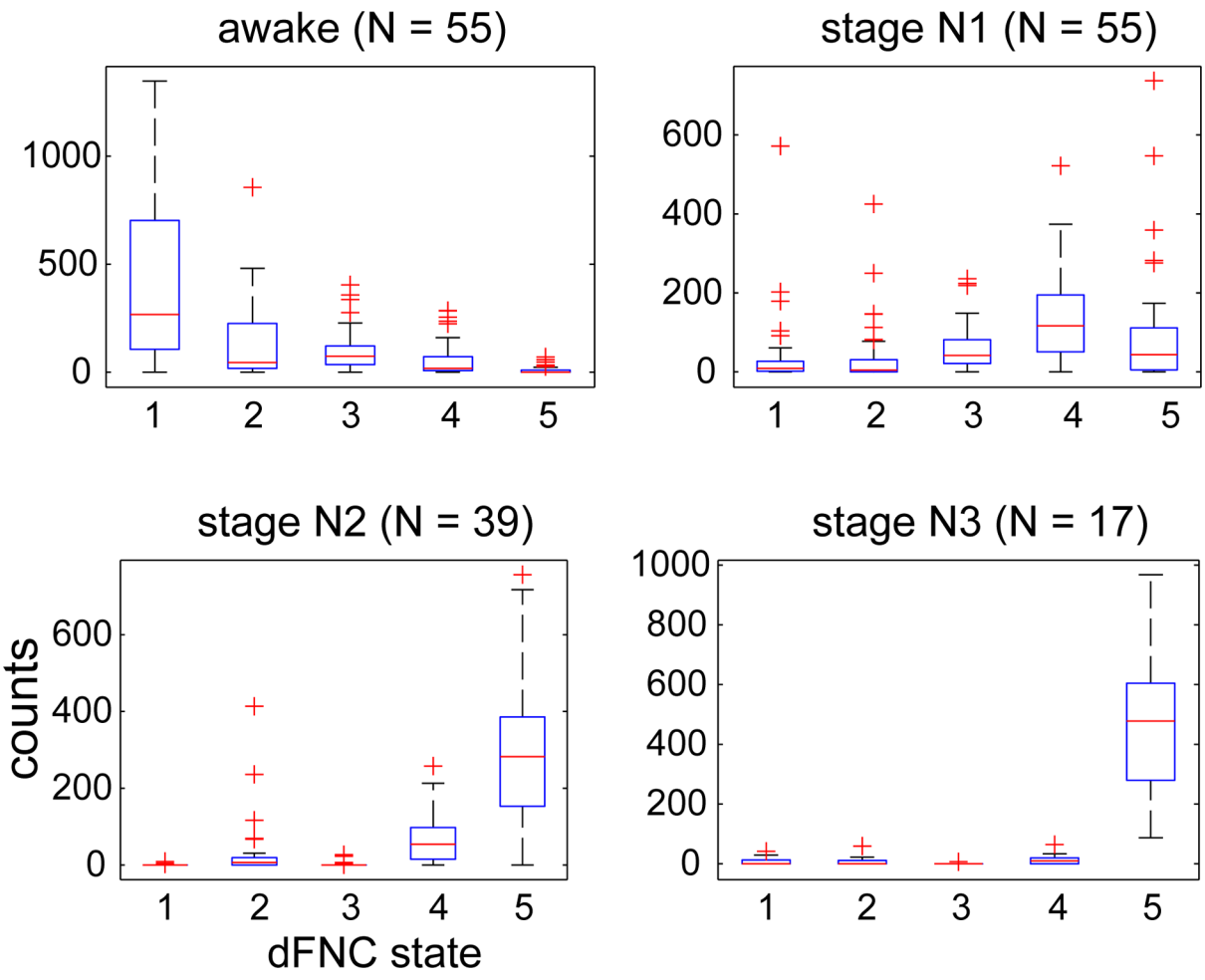

Figure 4:
Frequency counts of state vector assignments obtained from k-means clustering of dFNC data sorted by hypnogram states. States 1 and 2 primarily occur during wakefulness, dFNC states 4 and 5 during N2 sleep stage and state 5 is predominant during deep sleep (N3 stage).

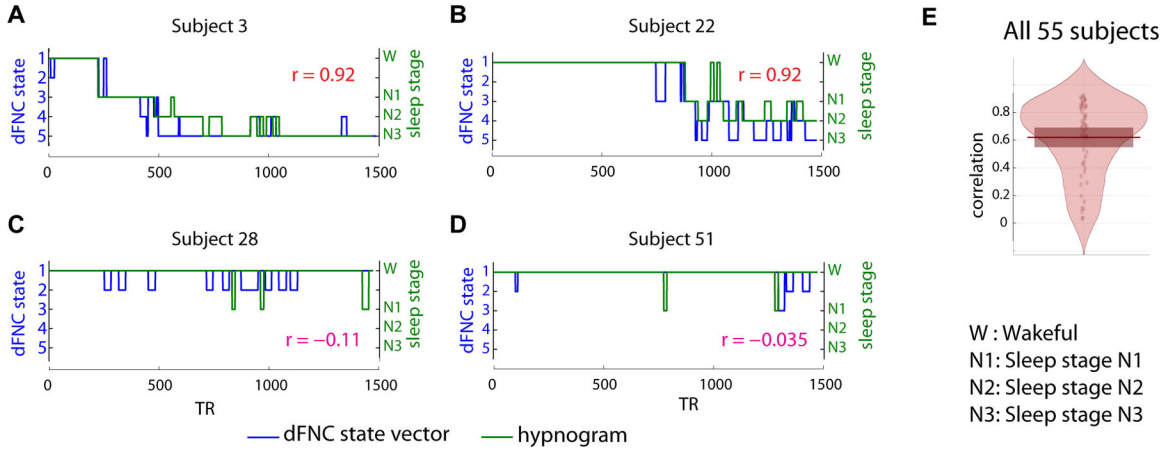

Figure 5:

Comparison of subject state vectors obtained from k-means clustering of dFNC windows and EEG derived hypnograms for the two subjects with the highest correlation (A and B) and the two subjects with the lowest correlation (C and D). The overall distribution of the correlation between the two state vectors for all 55 subjects is presented in E. As seen, the subjects with low correlation tend to be awake throughout the scan session and the corresponding dFNC state vector transitions within the states 1 and 2 that are prevalent during wakefulness.

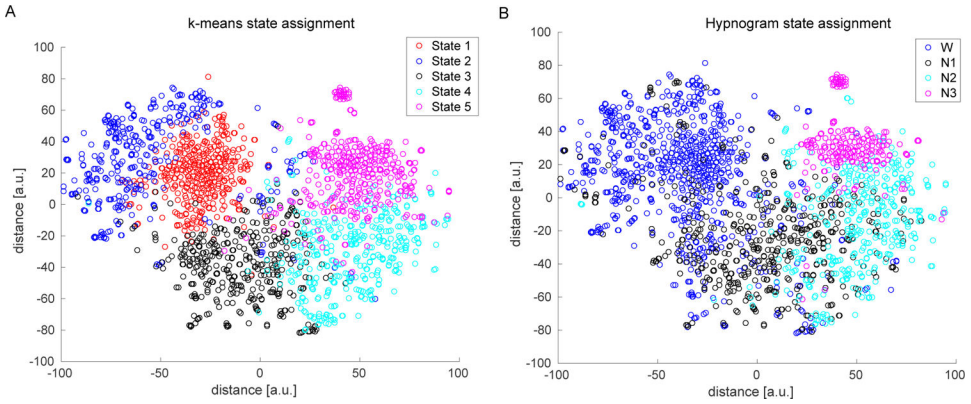

Figure 6:

2D Visualization of dFNC data: We selected 2000 random dFNC windows (400 per dFNC state) and projected the multidimensional (1891) data into 2 dimensions using the t-SNE algorithm. The resulting mapping was subsequently color coded by k-means clustering assignment into 5 states (A) and by the subject EEG hypnogram state of that point (B). The data dimension was reduced to 30 principal components and a perplexity value of 35 was used for this projection.

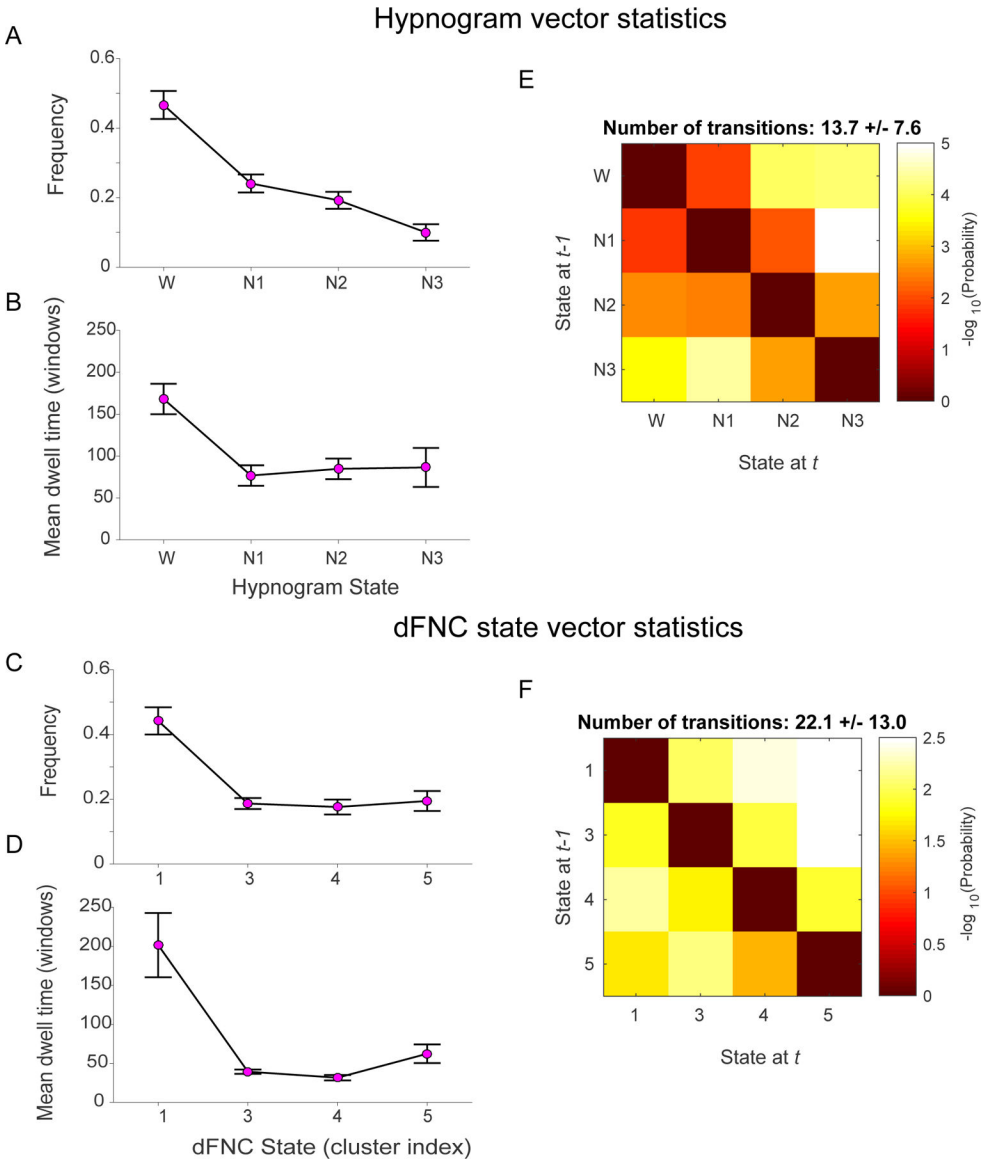

Figure 7:

Comparison of state vector statistics and transition matrices computed from EEG-derived hypnograms and dFNC cluster derived subject state vectors. Hypnogram and dFNC state vector exhibit similar frequency of occurrences (A and C) and mean dwell times (C and D) respectively. The mean state transition matrices for hypnogram vectors (E) and dFNC state vectors (F) inform about the probability of transitioning from a given state *i* at time t-1 to state *j* at time t. The probabilities are converted to -log(10) scale, so higher (yellow to white) intensity values mean lower probability to transition. For both modalities, these matrices demonstrate tendency to remain in a given state (diagonal values are lower). The transitions to neighboring states are more likely in both the hypnogram and the dFNC state vectors. While there is chance of transitioning from deep sleep N3 to any other state (W, N1 or N2), the probability of transitioning from wakefulness at time t-1 immediately to deeper sleep

stages (N2, N3) at time t is very low suggesting gradual transition from W to N3 stage. Note that dFNC states 1 and 2 are combined for this analysis.

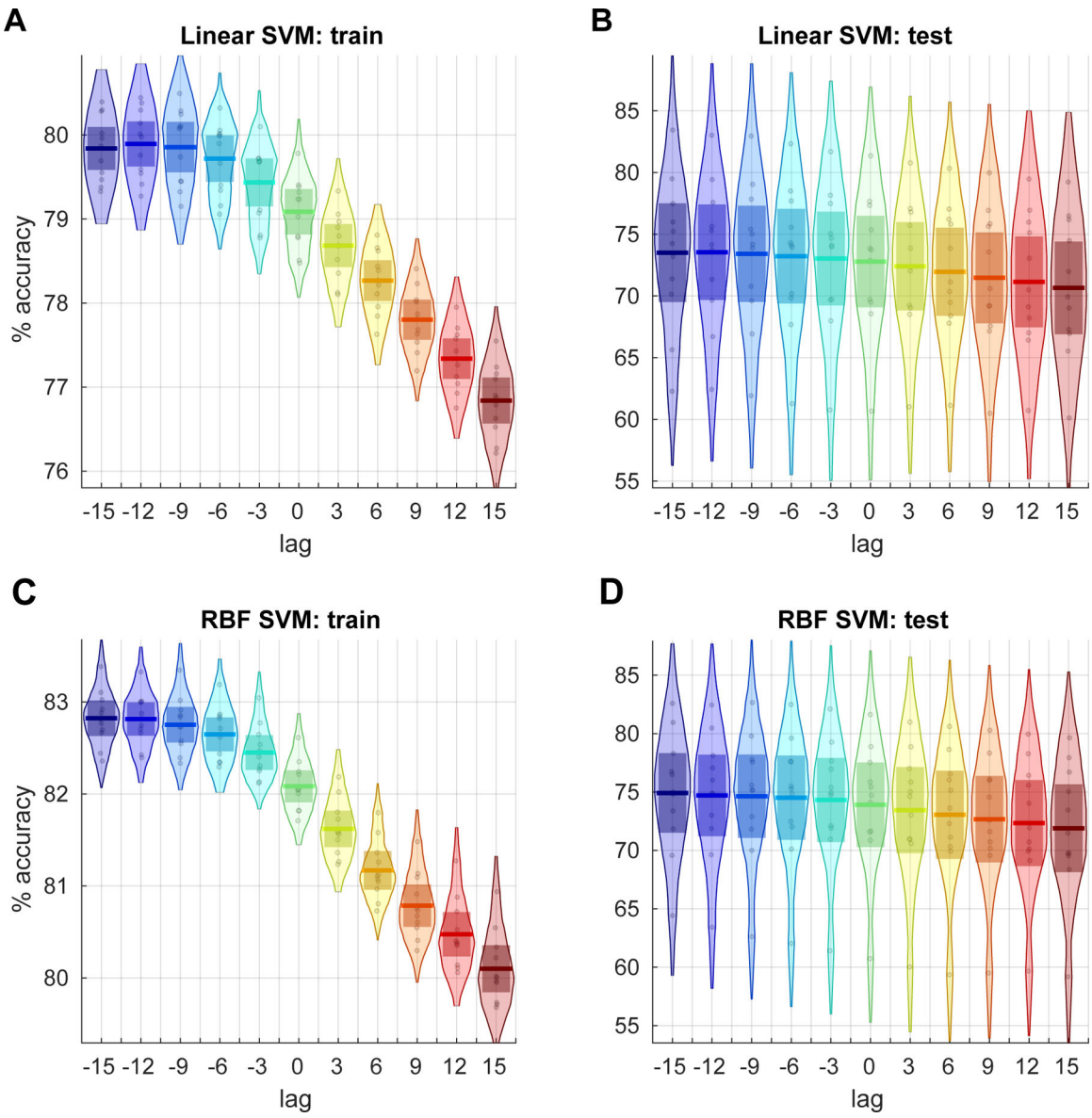

Figure 8:

Classification accuracies using linear SVM for training (A) and test (B) cases of alignment between EEG hypnogram and subject dFNC state vector obtained using a window size of 30 TRs. The alignment is tested for lags −15 to 15 TRs in step of 3 TRs. Each point in the distribution corresponds to the balanced per class accuracy from one of the 11 cross-validation iterations of training data that included data from 50 random subjects and the accuracy from left of test data that included data from 5 remaining subjects. The results using a SVM with RBF kernel for the same data are shown in C and D. Results are consistent for both linear and RBF SVM kernels .

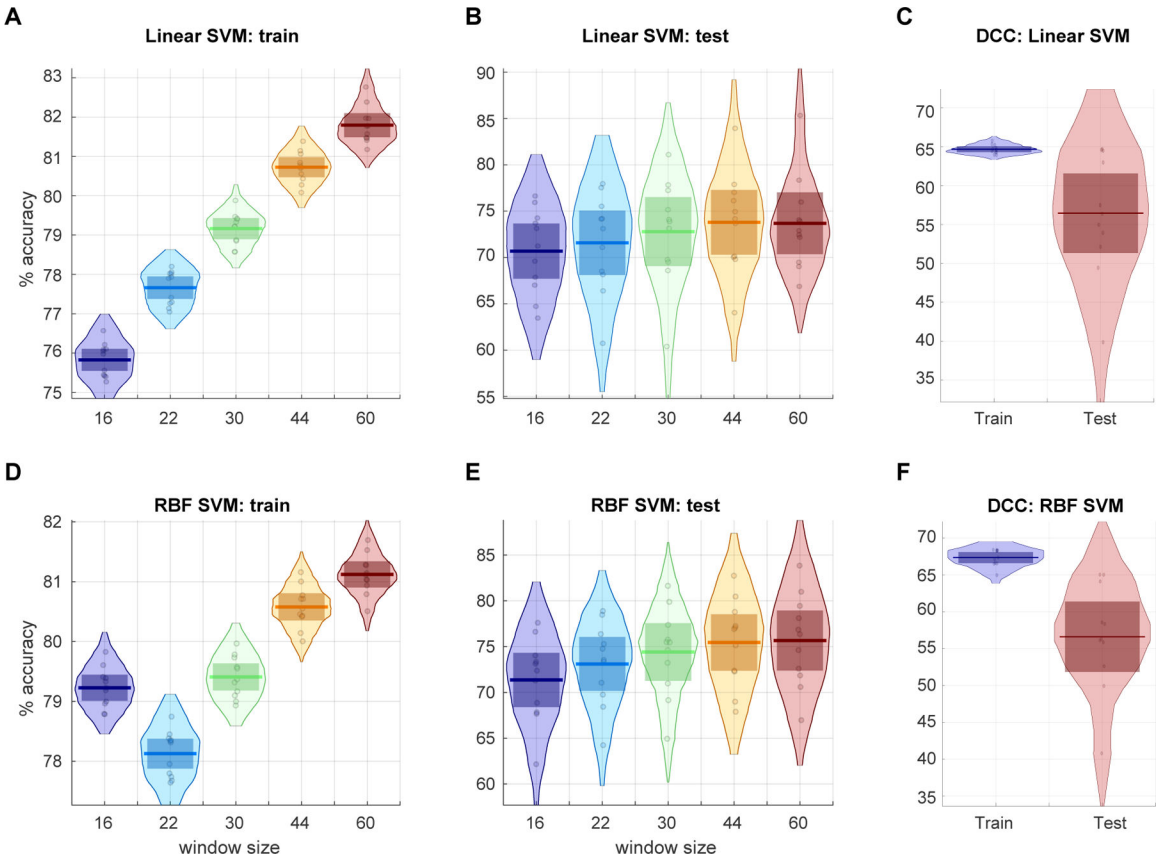

Figure 9:

Linear SVM classification accuracies of subject sleep stage from dFNC estimates obtained using different window sizes for training (A), test (B) data from 11 cross-validation iterations and the classification accuracies obtained from the DCC estimates for the same cross-validation scheme for training and left out test data are presented in the top right (C). The classification accuracies obtained with RBF kernel for the train (D), test(E) dFNC estimates and for DCC estimates (F) are shown.

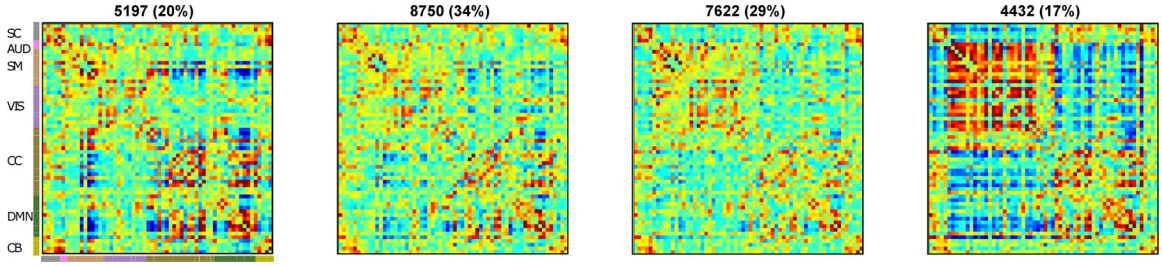

Figure 10:

Cluster centroids from k-means clustering of window dFNC data of awake only state (State 1). The estimated clusters were observed to have meaningful and distinct structure.

Table 1:

Peak activations of ICN SMs.

The quality index (I_q) associated with each ICN is listed in parentheses adjacent to the component number; V_ℓ = number of voxels in each cluster; t_{max} = maximum t-statistic in each cluster;Coordinate = coordinate (in mm) of t_{max} in MNI space, following LPI convention.

Subcortical Networks	V_ℓ	t_{max}	**Coordinate**
IC 58 (0.97)			
R Caudate Nucleus	626	52.15	18 −16 20
IC 27 (0.98)			
R Caudate Nucleus	786	66.366	12 14 8
IC 91 (0.76)			
L Putamen	342	87.587	−21 8 −7
R Putamen	338	92.203	24 11 −7
IC 98 (0.68)			
R Putamen	372	94.022	27 −1 2
L Putamen	359	113.49	−27 −4 2
IC 20 (0.98)			
R Thalamus	861	87.008	6 −13 5
Auditory Networks	V_ℓ	t_{max}	**Coordinate**
IC 34 (0.98)			
R Insula Lobe	438	48.445	33 −25 17
L Rolandic Operculum	415	42.729	−45 −22 11
IC 14 (0.98)			
R Superior Temporal Gyrus	347	46.328	60 −16 −4
L Superior Temporal Gyrus	303	35.198	−60 −13 2
Sensorimotor Networks	V_ℓ	t_{max}	**Coordinate**
IC 2 (0.98)			
L Postcentral Gyrus	229	52.196	−48 −10 32
R Postcentral Gyrus	221	53.635	57 −4 29
IC 4 (0.98)			
R Precentral Gyrus	570	71.156	36 −22 53
IC 7 (0.98)			
L Postcentral Gyrus	595	65.889	−36 −25 56
IC 81 (0.9)			
R Middle Cingulate Cortex	815	52.287	3 −7 47
IC 3 (0.98)			
R Paracentral Lobule	728	57.783	3 −28 68
IC 55 (0.97)			
R Postcentral Gyrus	416	46.245	54 −19 35
L Postcentral Gyrus	292	39.467	−60 −22 29
IC 80 (0.95)			

Subcortical Networks	V_ℓ	t_{max}	**Coordinate**
L Superior Frontal Gyrus	855	42.788	−21 −4 65
IC 67 (0.96)			
L Superior Parietal Lobule	431	48.987	−21 −49 68
R Superior Parietal Lobule	332	45.144	15 −49 65
IC 26 (0.98)			
R Middle Temporal Gyrus	267	50.626	51 −67 2
L Middle Occipital Gyrus	171	39.173	−45 −70 5
IC 48 (0.98)			
R Precentral Gyrus	334	52.234	21 −22 59
L Precentral Gyrus	150	45.439	−21 −25 59
Visual Networks	V_ℓ	t_{max}	**Coordinate**
IC 77 (0.92)			
L Lingual Gyrus	719	52.696	−18 −73 −10
IC 17 (0.98)			
L Cuneus	932	63.044	−3 −85 38
IC 11 (0.98)			
R Calcarine Gyrus	1133	61.631	15 −67 8
IC 25 (0.98)			
L Calcarine Gyrus	752	64.739	3 −85 2
IC 38 (0.97)			
R Fusiform Gyrus	320	52.29	30 −49 −10
L ParaHippocampal Gyrus	226	48.254	−27 −43 −10
IC 97 (0.73)			
R Lingual Gyrus	972	43.732	18 −73 −7
IC 66 (0.95)			
L Cuneus	939	46.324	−6 −97 14
IC 22 (0.98)			
R Lingual Gyrus	674	51.127	21 −94 −7
IC 69 (0.94)			
R Middle Occipital Gyrus	384	53.579	42 −73 35
L Middle Occipital Gyrus	218	37.83	−39 −76 32
IC 73 (0.94)			
L Superior Occipital Gyrus	375	44.761	−24 −73 35
R Middle Occipital Gyrus	191	42.562	33 −73 23
IC 50 (0.97)			
R Inferior Occipital Gyrus	349	40.302	45 −73 −10
L Lingual Gyrus	264	36.962	−33 −85 −16
Cognitive Control Networks	V_ℓ	t_{max}	**Coordinate**
IC 76 (0.91)			
R Inferior Parietal Lobule	602	52.132	39 −40 50
IC 71 (0.95)			
L Inferior Parietal Lobule	552	53.538	−45 −37 44

Subcortical Networks	V_ℓ	t_{max}	Coordinate
IC 42 (0.97)			
L Inferior Temporal Gyrus	331	53.568	−57 −58 – −7
R Middle Temporal Gyrus	151	37.405	60 −52 −7
IC 84 (0.88)			
R Inferior Temporal Gyrus	568	41.245	45 −13 −25
IC 60 (0.95)			
L Postcentral Gyrus	272	49.711	−48 −13 47
R Precentral Gyrus	260	43.566	45 −10 41
IC 63 (0.96)			
L Insula Lobe	324	44.285	−36 2 11
R Insula Lobe	264	52.788	36 5 11
IC 74 (0.93)			
L Anterior Cingulate Cortex	668	51.736	−3 26 26
IC 47 (0.97)			
L Angular Gyrus	583	48.228	−42 −70 41
IC 65 (0.94)			
L Inferior Frontal Gyrus (p. Opercularis)	396	42.552	−42 11 29
R Inferior Frontal Gyrus (p. Opercularis)	96	29.433	42 14 32
IC 89 (0.92)			
L Inferior Frontal Gyrus (p. Opercularis)	465	40.334	−54 14 8
R Inferior Frontal Gyrus (p. Triangularis)	213	35.37	54 26 5
IC 53 (0.96)			
R Insula Lobe	421	50.671	36 20 −1
L Insula Lobe	305	47.124	−33 17 8
IC 33 (0.98)			
R SupraMarginal Gyrus	286	44.455	57 −46 35
L Inferior Parietal Lobule	278	44.221	−54 −49 38
IC 32 (0.98)			
R Superior Orbital Gyrus	288	37.454	27 56 −1
L Middle Frontal Gyrus	274	33.346	−30 53 2
IC 51 (0.97)			
R Middle Frontal Gyrus	397	43.207	30 44 29
L Middle Frontal Gyrus	280	34.033	−33 38 29
IC 49 (0.98)			
R Inferior Temporal Gyrus	328	40.668	63 −31 −19
L Middle Temporal Gyrus	259	38.391	−63 −43 −13
IC 86 (0.86)			
R Middle Frontal Gyrus	715	49.803	27 17 53
L Middle Frontal Gyrus	166	33.725	−27 23 53
IC 78 (0.95)			
L SMA	673	57.132	−3 11 62
IC 36 (0.98)			

Subcortical Networks	V_ℓ	t_{max}	**Coordinate**
R Superior Temporal Gyrus	547	44.804	57 −49 20
IC 96 (0.69)			
R Inferior Frontal Gyrus (p. Triangularis)	199	39.597	42 35 17
R Inferior Frontal Gyrus (p. Opercularis)	110	30.408	51 11 23
Default-mode Networks	V_ℓ	t_{max}	**Coordinate**
IC 18 (0.98)			
R Middle Cingulate Cortex	134	45.344	3 −22 29
R Precuneus	93	41.094	12 −64 35
IC 75 (0.95)			
R Precuneus	738	59.873	3 −52 50
IC 83 (0.89)			
L Precuneus	687	52.332	0 −64 59
IC 13 (0.98)			
L Precuneus	532	60.221	−6 −52 14
IC 59 (0.97)			
L Middle Cingulate Cortex	735	59.744	−3 −31 35
IC 61 (0.95)			
R Inferior Parietal Lobule	539	50.287	45 −58 50
IC 57 (0.96)			
L Mid Orbital Gyrus	851	44.422	0 50 −13
IC 24 (0.98)			
L Precuneus	443	81.554	0 −61 32
IC 35 (0.97)			
L Superior Medial Gyrus	885	43.348	−3 47 35
IC 29 (0.98)			
L Middle Temporal Gyrus	591	41.693	−51 −52 14
Cerebellar Networks	V_ℓ	t_{max}	**Coordinate**
IC 16 (0.98)			
R Cerebellum (Crus 1)	1198	50.811	18 −76 −28
IC 100 (0.61)			
L Cerebellum (Crus 1)	201	30.986	−36 −46 −34
IC 45 (0.97)			
R Cerebellum (VI)	568	42.816	30 −49 −34
IC 8 (0.98)			
R Cerebellum (IX)	837	48.11	15 −58 −49
IC 9 (0.98)			
R Cerebellum (IV-V)	987	62.466	12 −49 −19

Table 2:

Awake state SVM classification confusion matrix.

The percent classification accuracy from RBF SVM model for each of the four awake only K-means states. The classification was performed using leave 5 subject out cross validation scheme and the average train (left) and test (right) confusion matrix across folds is shown above. The high accuracy strongly suggests that these clusters are unlikely to be noise.

		Train:Predicted				Test:Predicted			
		AwState 1	**AwState 2**	**AwState 3**	**AwState 4**	**AwState 1**	**AwState 2**	**AwState 3**	**AwState 4**
Actual	AwState 1	95.8	2.31	1.8	0.09	91.28	4.44	3.36	0.92
	AwState 2	0.63	97.54	1.36	0.47	1.51	93.42	3.74	1.33
	AwState 3	0.77	2.09	96.07	1.08	2.4	3.44	92.14	2.02
	AwState 4	0.3	1.07	2.12	96.52	1.7	2.3	3.95	92.03